Hierarchical alignment of breast DCE-MR images by groupwise registration and robust feature matching

Minjeong Kim, Guorong Wu, and Dinggang Shen[a)]
Department of Radiology and BRIC, University of North Carolina, Chapel Hill, North Carolina 27599

(Received 22 April 2011; revised 5 October 2011; accepted for publication 10 November 2011; published 22 December 2011)

Purpose: Dynamic contrast-enhanced magnetic resonance imaging (DCE-MRI) shows high sensitivity in detecting breast cancer. However, its performance could be affected by patient motion during the imaging. To overcome this problem, it is necessary to correct patient motion by deformable registration, before using the DCE-MRI to detect breast cancer. However, deformable registration of DCE-MR images is challenging due to the dramatic contrast change over time (especially between the precontrast and postcontrast images). Most existing methods typically register each postcontrast image onto the precontrast image independently, without considering the dynamic contrast change after agent uptake. This could lead to the inconsistency among the aligned postcontrast images in the precontrast image space, which will eventually result in worse performance in cancer detection. In this paper, the authors present a novel hierarchical registration framework to address this problem.

Methods: First, the authors propose a hierarchical registration framework to deploy the groupwise registration for simultaneous registration of all postcontrast images onto their group-mean image and further aligning the group-mean image of postcontrast images onto the precontrast image space for final alignment of all precontrast and postcontrast images. In this way, the postcontrast images (with similar intensity patterns) can be jointly aligned onto the precontrast image for increasing their overall consistency after registration. Second, in order to improve the registration between the precontrast image and the group-mean image of the postcontrast images, the authors propose using the contrast-invariant attribute vectors to guide the robust feature matching during the registration.

Results: Our proposed hierarchical registration framework has been comprehensively evaluated and compared with affine registration and widely used deformable registration methods in both pairwise and groupwise registration formulation. The experimental results on both real and simulated images show that our method can obtain not only more accurate but also more consistent registration results than any of all other registration algorithms.

Conclusions: The authors have proposed a novel groupwise registration method to achieve accurate and consistent alignment for breast DCE-MR images. In the future, the authors will further evaluate our proposed method with more clinical datasets. [DOI: 10.1118/1.3665705]

Key words: dynamic contrast-enhanced (DCE) MRI, feature-based deformable registration, breast tumor image, groupwise registration, local steering kernel

I. INTRODUCTION

DCE-MRI, termed as dynamic contrast-enhanced magnetic resonance imaging, is a widely used imaging protocol in the diagnosis of breast tumor. After injection of contrast agent, the patterns between benign and malignant tumors in the DCE-MR image behave differently, as can be reflected by the wash-in and wash-out curves of the contrast agent. As Refs. 1 and 2 show, the intensity around carcinoma (malignant tumor) in DCE-MR image increases rapidly at the first and second postcontrast time points and then decreases gradually at subsequent time points. In contrast, the curve of the fibroadenoma (benign tumor) keeps increasing after injection. Therefore, the consistent point-by-point comparison of intensity change over time between the precontrast image (before contrast injection) and postcontrast images (after contrast injection) is important for the classification between benign and malignant tumors.

Accordingly, the precontrast and postcontrast images should be well aligned in a common space (usually the precontrast image space) before using them to detect tumors. However, the conventional optical flow-based methods,[3,4] which assume the intensities to be constant in the precontrast and postcontrast images, might not be able to correct the entire patient motion because of the nonuniform intensity change. To this end, many deformable registration methods, parameterized by local transformation models, have been investigated to more accurately align the DCE-MR images, e.g., using the normalized mutual information as a cost function and modeling the deformation field by B-splines,[5–7] multiscale fluid model,[8] or finite element model (FEM).[9,10] However, these intensity-based registration methods still suffer from the dramatic intensity change between precontrast and postcontrast images, which could introduce some artifacts

after registration, especially around tumor area. For example, as reported in Refs. (11 and 12), the dramatic contrast change could result in the unrealistic shrinkage or expansion of tumor after registration. To alleviate this issue, the concept of volume preserving registration[11,12] is introduced to the B-spline-based free-form deformation framework to enforce the incompressibility of tumor region.

Many methods have been proposed to address the problem of dramatic contrast change in DCE-MR images by explicitly estimating the enhanced contrast after agent injection when registering the precontrast and postcontrast images. For example, several methods in Refs. 13–15 introduce the brightness shift term in the optical flow equation to account for the dynamic intensity changes. Besides, an iterative optimization algorithm has also been presented in Ref. 16 to de-enhance the breast DCE-MR images and then to register precontrast and postcontrast images for avoiding the dynamic intensity changes. Recently, Zheng *et al.*[17] further proposed to use the *Lorentzian* estimator, which is the log function of time, to handle the temporal intensity change.

However, the existing breast DCE-MR image registration algorithms are limited at several aspects. (1) Most algorithms only use image intensity to drive the registration. However, the matching of image intensities does not necessarily mean the correct anatomical correspondences. (2) The large contrast difference between the two underlying images is not considered during the image registration. Although some methods can manage to make the contrast as similar as possible before registration, the solutions have not been fully incorporated into the registration. (3) The registrations are independently performed between precontrast image and each of the postcontrast images, thus possibly leading to inconsistent registration among all postcontrast images. This may lead to discontinuous intensity change over time, while the intensities in the real tumor should be smoothly evolved according to the wash-in and wash-out curves.

It is clear that the key to achieve accurate and consistent registration is to resolve the difficulty in the large contrast difference among a series of DCE-MR images. In this paper, we present a novel hierarchical registration framework for breast DCE-MR images. We observe that the intensity variations among all postcontrast images are much smaller than those between precontrast and postcontrast images. In other words, the registration between the postcontrast images is much less challenging than that between precontrast and postcontrast image pair. In light of this, we propose to solve the registration problem in a divide-and-conquer way, which consists of two steps. In the *first* step, we propose to employ groupwise registration on all postcontrast images. Thus, we are able to gain reliable and consistent alignment of these postcontrast images. Here, we follow the unbiased groupwise registration approach which iteratively (1) estimates the group-mean image according to the current registration results and (2) registers all postcontrast images to the latest estimated group-mean image. In the *second* step, we propose a robust feature-based, instead of only intensity-based, registration method to align the group-mean image of all postcontrast images with the precontrast image. Specifically, two kinds of image features, i.e., local histogram (LH) and local steering kernel (LSK), are utilized, which work in intensity and gradient domains, respectively. In particular, the LSK (Ref. 18) estimated from the covariance matrix of local gradients is robust to the contrast change[19] since it captures the local variations of boundary. On the other hand, the local histogram based feature, measuring the regional intensity changes, is less sensitive to the image noise than the gradient-based features. After combining these two image features, we follow the hierarchical deformation strategy used in our previous work[20] to establish the reliable correspondences between precontrast and postcontrast images. By registering all postcontrast images and precontrast image in these two steps, we can achieve much better registration results in terms of registration accuracy and consistency. We have comprehensively evaluated the performance of our proposed registration method on both simulated and real breast DCE-MR images, with the comparison to affine registration, free-form deformation (FFD)[5] method with volume-preserving constraint, hierarchical attribute-based registration algorithm (HAMMER),[20] in both pairwise and groupwise formulation. In all experiments, our proposed method outperforms all other algorithms, thus demonstrating the advantage of our hierarchical groupwise registration framework.

In the following, we first present the details about our proposed registration method in Sec. II. Then, we evaluate our proposed method in Sec. III by comparison with affine registration, three pairwise registration, and three groupwise registration methods. Finally, we make a conclusion in Sec. IV.

II. METHODS

We will first present the overview of our hierarchical registration framework for breast DCE-MR images in Sec. II A. Then, we will describe the groupwise registration of all postcontrast images in Sec. II B, followed by the registration between the precontrast image and the group-mean image of all postcontrast images by a robust feature matching algorithm in Sec. II C. Finally, we will summarize our overall registration framework for the breast DCE-MR images in Sec. II D.

II.A. The overview of our hierarchical registration framework

The goal of the registration on a DCE-MR image sequence is to align all N postcontrast images $I_t(t = 1, \ldots, N)$ to the domain of precontrast image I_0 by estimating the dense deformation fields $F_t = \{f_t(x)|f_t(x) = x + u_{I_0 \to I_t}(x), x \in \Omega_{I_0}\}$, where $u_{I_0 \to I_t}(x)$ denotes the displacement of a point x in the precontrast image domain Ω_{I_0} to the postcontrast image I_t. After injecting the agent, the contrast around tumor area greatly increases in the first few minutes and then the intensity change becomes stable in the following postcontrast stage. As shown in Fig. 1, the histograms of N postcontrast images look very similar to each other, but all of them are quite different from the precontrast image. It is worth noting that all the conventional methods [as illustrated in Fig. 1(a)] overlook this phenomena by simply registering each postcontrast image

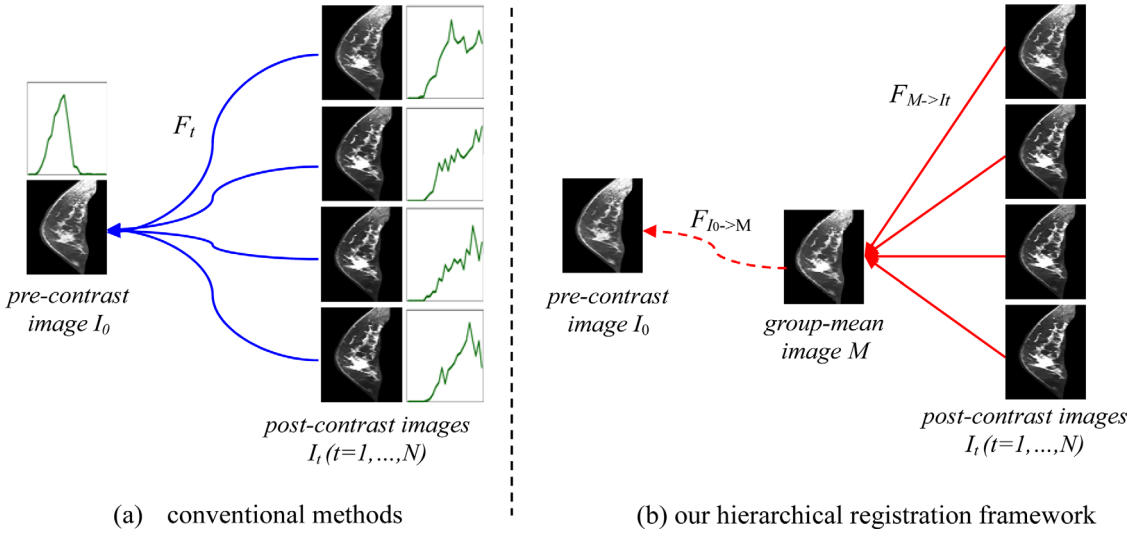

FIG. 1. Illustration of the conventional pairwise registration approach (a) and the proposed hierarchical registration framework (b).

independently with the precontrast image. As mentioned earlier, the registration between precontrast image and any postcontrast image is extremely challenging due to the dramatic contrast change. Also, by registering each postcontrast image to the precontrast image independently, the temporal consistency of all aligned postcontrast images in the precontrast image space cannot be guaranteed, which will eventually affect the measurement of dynamic contrast change in different parts of breast that is important for the diagnosis of breast cancer.

Accordingly, we propose a hierarchical registration framework [as described in Fig. 1(b)] to overcome these limitations in two steps. In the *first* step (SP_1: groupwise registration upon all postcontrast images), we consider all postcontrast images as a whole and deploy a groupwise registration algorithm to jointly register them onto their common space, i.e., a group-mean image space. Since the contrasts among all postcontrast images are similar, more reliable registration results can be achieved. As we will make it clear in Sec. II B, the group-mean image M and the intermediate deformation field $F_{M\to I_t} = \{f_{M\to I_t}(x) | f_{M\to I_t}(x) = x + u_{M\to I_t}(x), x \in \Omega_M\}$ [i.e., the solid arrows in Fig. 1(b)] of all I_t toward the common space can be jointly obtained at the end of groupwise registration. In the *second* step (SP_2: registration between the precontrast image and the group-mean image), we propose a robust feature-based registration algorithm to estimate the deformation field from the precontrast image I_0 to group-mean image M, denoted as $F_{I_0\to M} = \{f_{I_0\to M}(x) | f_{I_0\to M}(x) = x + u_{I_0\to M}(x), x \in \Omega_{I_0}\}$ [see the red dashed arrow in Fig. 1(b)]. Specifically, we use the attribute vector as the morphological signature to establish the reliable anatomical correspondences between M and I_0. The difficulties lying here are the image noise as well as the contrast change between I_0 and M. Here, we use local histogram and local steering kernel based features as the attribute vector of each point to deal with these problems. As we will demonstrate later, more robust registration results can be achieved by integrating this attribute vector in our registration. Finally, the deformation field F_t of the precontrast image to each postcontrast image can be composed by the deformation fields $F_{I_0\to M}$ and $F_{M\to I_t}$, i.e., $F_t = F_{M\to I_t} \circ F_{I_0\to M}$.

Compared with the conventional registration methods, our hierarchical registration framework has the following advantages: (1) The registration consistency can be well preserved by considering all postcontrast images jointly; (2) the registration accuracy can be better achieved by robust feature matching between the group-mean and the postcontrast images. These two points will be made clear in Secs. II B–II C.

II.B. Groupwise registration on postcontrast images

The goal of this step is to register all postcontrast images I_t to the common space by jointly estimating the deformation field $F_{M\to I_t}$ and the group-mean image M. We follow the unbiased groupwise registration method[21], which has two iterative steps: Step 1: Compute the group-mean image based on current registration results; Step 2: Register all images to the latest group-mean image by a pairwise registration algorithm.

Suppose that in the end of $(k-1)$th iteration, each postcontrast image I_t has been deformed as I_t^{k-1} w.r.t its current estimated deformation field $F_{M\to I_t}^{k-1}$, where $I_t^{k-1}(x) = I_t(F_{M\to S_t}^{k-1}(x))$. Then in the next iteration (k th iteration), the mean image M^k can be updated as

$$M^k(x) = \frac{1}{N}\sum_{i=1}^{N} I_i^{k-1}(x). \quad (1)$$

After that, each postcontrast image I_t needs to register with M^k by pairwise registration (i.e., with the method presented in Sec. II C), thus obtaining its new deformation field $F_{M\to I_t}^k$ for the next iteration [$(k+1)$ th]. In the end of groupwise registration, the group-mean image M in the common space can be obtained, as well as the deformation field $F_{M\to I_t}$ of each postcontrast image I_t.

Although many existing intensity-based registration algorithms can be deployed in step 2, they may still suffer from

the contrast difference between the group-mean image and each postcontrast image. In our point of view, a good registration method needs to (1) Establish the correct correspondences for the DCE-MR images with dramatic contrast changes and image noise; (2) Avoid overdeformation of breast tumor which keeps relatively rigid during the breast motion. Although some methods have been proposed to handle the rigid transformation of tumor during registration,[11,22–26] they usually incorporate the tumor motion constraint by a specified regularization term, e.g., using Jacobian determinant to force the local volume incompressibility.

In Sec. II C, we will present our robust feature-based registration method for DCE-MR images, which is used in both the registration of all postcontrast images and their group-mean image in SP_1 and the registration between the precontrast image and the group-mean image of all postcontrast images in SP_2.

It is worth noting that we will use T to denote the template image and S for the subject image in Sec. II C. In SP_1, i.e., the groupwise registration of all postcontrast images, each postcontrast image I_t needs to align with the currently estimated group-mean image M^k at each iteration k. Thus, we use M^k as the template T and also I_t as subject S in the registration method described below. In SP_2, we will register the precontrast image I_0 with the group-mean image M of all postcontrast images. Therefore, in this case, we will use I_0 as the template T and also M as the subject.

II.C. Robust feature-based registration for DCE-MR images

In our registration method, we establish robust anatomical correspondences in two ways. First, we define an attribute vector as the morphological signature for each point to characterize its geometric information in the neighborhood. Second, we hierarchically select a set of points with distinctive attribute vectors to drive the registration of the whole images, thus better avoiding the ambiguity in image matching. Moreover, we treat tumor motion as rigid motion by fitting rigid transformation to the estimated nonrigid deformation around the tumor area. In the following, we will first detail these two strategies and then present the energy function and its solution for our deformable registration method.

II.C.1. Attribute vector

The attribute vector on each point x consists of three components, which can be represented as $\bar{a}(x) = [a^{\text{Bound}}(x), \bar{a}^{\text{Hist}}(x), \bar{a}^{LSK}(x)]$. Here, $a^{\text{Bound}}(x)$ is a scalar value denoting the boundary response by the Canny edge detector.[27] $\bar{a}^{\text{Hist}}(x)$ denotes a set of low-order geometric moments on local intensity histogram, computed from a spherical region of point x with radius r. Here, we use the zeroth-, first-, and second-order geometric moments. It is worth noting that $\bar{a}^{\text{Hist}}(x)$ has been normalized between 0 and 1. Thus, given a point x in the template T and another point y in the subject image S, the similarity of their histogram-based features can be defined as

$$m_{\text{Hist}}\left(\bar{a}_T^{\text{Hist}}(x), \bar{a}_S^{\text{Hist}}(y)\right) = \prod\nolimits_j \left(1 - |a_{T,j}^{\text{Hist}} - a_{S,j}^{\text{Hist}}(y)|\right), \quad (2)$$

where $a_{T,j}^{\text{Hist}}(x)$ and $a_{S,j}^{\text{Hist}}(x)$ are the jth element of LH-based attribute vector of the template and subject images, respectively.

The histogram-based features $\bar{a}^{\text{Hist}}(x)$ are rotation-invariant and robust to image noise, however, they are not invariant to contrast change, which is the main challenge in the registration of DCE-MR images. To overcome this difficulty, we introduce the LSK as the complementary attribute vector to deal with the contrast change. In brief, LSK-based feature is computed by the following three steps: (i) the $D \times D$ (i.e., $D = 2$ in 2D image and $D = 3$ in volumetric image) covariance matrix $C(x)$ of gradients is first calculated from a $P \times P$ local patch around each point x; (ii) an LSK-based attribute vector of the point x is defined from a $Q \times Q$ window centered at x as $\bar{a}^{LSK}(x) = [LSK(x_i - x, C(x_i)), i = 1, \ldots, Q^2]$, where x_i denotes a point in the $Q \times Q$ window. Each element $LSK(x_i - x, C(x_i))$ is obtained by:

$$LSK(x_i - x, C(x_i)) = \frac{\sqrt{\det(C(x_i))}}{h^2} \exp\left(-\frac{(x - x_i)' C(x_i)(x - x_i)}{2h^2}\right) \quad (3)$$

where h denotes the kernel width and $\det(C(x_i))$ returns the determinant value of covariance matrix $C(x_i)$. The principle behind Eq. (3) is that the local geometric structure is implicitly encoded by the intensity differences (i.e., gradients in $P \times P$ local patch), which characterizes the shape and size of canonical kernel; (iii) $\bar{a}^{LSK}(x)$ needs to be normalized within the $Q \times Q$ window. Therefore, each element $LSK(x_i - x, C_i)$ after normalization is given as

$$LSK(x_i - x, C(x_i)) \leftarrow \frac{LSK(x_i - x, C(x_i))}{\sum_{i=1}^{Q^2} LSK(x_i - x, C(x_i))} \quad (4)$$

The examples of LSK on three pairs of correspondences (pink boxes) between template (a) and subject image (b) are demonstrated in Fig. 2, with their LSK features displayed in the color maps. It can be observed that the patterns of LSK are quite unique in different locations of the image. Also, the LSK in the template image is similar only to its correspondence in the subject image, which indicates its ability for correspondence detection in the registration.

We use the cosine similarity measure[19] to evaluate the similarity between template point x and subject point y as

$$m_{LSK}\left(\bar{a}_T^{LSK}(x), \bar{a}_S^{LSK}(y)\right) = \left\langle \frac{\bar{a}_T^{LSK}(x)}{\left\|\bar{a}_T^{LSK}(x)\right\|}, \frac{\bar{a}_S^{LSK}(y)}{\left\|\bar{a}_S^{LSK}(y)\right\|} \right\rangle = \frac{\bar{a}_T^{LSK}(x) \cdot \bar{a}_S^{LSK}(y)}{\left\|\bar{a}_T^{LSK}(x)\right\| \cdot \left\|\bar{a}_S^{LSK}(y)\right\|}. \quad (5)$$

In this way, the overall similarity measurement between $\bar{a}(x)$ in the template and $\bar{a}(y)$ in the subject can be combined as

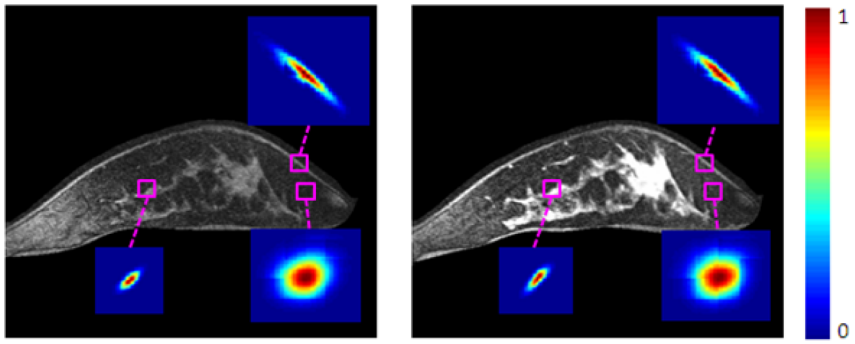

FIG. 2. The LSK on three pairs of correspondences between template (a) and subject (b). As can be observed, the kernel shapes between the corresponding points are more similar that other non-corresponding points, indicating the good discrimination ability of LSK in image registration.

$$m(\bar{a}_T(x),\bar{a}_S(y)) = \left((1-|a_T^{\text{Bound}}(x)-a_S^{\text{Bound}}(y)|)\right) \times \left[\lambda\cdot m_{\text{Hist}}\left(\bar{a}_T^{\text{Hist}}(x),\bar{a}_S^{\text{Hist}}(y)\right) +(1-\lambda)\cdot m_{LSK}\left(\bar{a}_T^{LSK}(x),\bar{a}_S^{LSK}(y)\right)\right], \quad (6)$$

where λ is used as the weight to balance between $\bar{a}^{\text{Hist}}$ and $\bar{a}^{LSK}$.

II.C.2. Driving points

Driving points (with distinctive attribute vectors) are used to help alleviate the ambiguity in correspondence matching and thus better avoid the local minima in registration.[20,28] Therefore, instead of determining the correspondence for each breast point, we perform the correspondence detection only on the driving points and let them guide the registration of other non-driving points. Here, we follow our previous work[20] to adaptively select the driving points by setting the threshold on the boundary attribute $a^{\text{Bound}}(x)$ on each point x. That is, N points with the large boundary values will be selected as the driving points, denoted as $DP = \{x_i^d | i = 1,\ldots,N\}$. As we will make it clear next, the selection of the driving point makes the energy function simple and allows only the critical points to drive the deformation during the image registration. With the progress of registration, more and more points will be selected as the driving points to join the registration of the images, and finally all points will be considered to drive the registration.

II.C.3. Energy function

The problem of image registration is usually solved by minimizing the energy function, which evaluates the similarity between two underlying images. In order to cast the deformable registration into the optimization of well-posed problem, we introduce the correspondence field $G = \{g(x)|x \in \Omega_T\}$ which only gives the corresponding location of template driving points $\{x_i^d\}$ in the subject image domain. Here, one advantage of using correspondence field G is that it decouples the complex optimization problem into two easy-to-conquer tasks,[29] i.e., establishing the correspondences $g(x_i^d)$ on the driving points and fitting the dense deformation field F w.r.t. correspondence field G with the smoothness regularization. The overall energy function used in our registration method between two DCE-MR images is

$$E(F,G) = \sum_{i=1}^{N}\sum_{v\in n(x_i^d)} m\left(\bar{a}_T(v),\bar{a}_S(g(v))\right) + \sum_{i=1}^{N}\left\|f(x_i^d)-g(x_i^d)\right\|^2 + \sigma\sum_x \|Lf(x)\|^2, \quad (7)$$

where $n(\cdot)$ denotes the small neighborhood of the underlying point. It is clear that the first term in the energy function measures the image similarity between template T and subject S; here, we only consider the driving points x_i^d, instead of all image points. In terms of robust feature matching, we measure not only the pointwise similarity but also the regionwise similarity in the neighborhood $n(x_i^d)$. The second term in Eq. (7) requires the correspondence detection results on the driving points should be spatially close to the previous estimated deformations. The last term is the widely used regularization term on the deformation field F with minimal bending energy.[30] The parameter σ controls the smoothness of the final deformation field F.

II.C.4. Optimization

The optimization of Eq. (7) is achieved by iteratively performing two steps, i.e., correspondence detection step and dense deformation field estimation step. By fixing the dense deformation F, the correspondence $g(x_i^d)$ on each driving point x_i^d can be solved by minimizing the first and second terms in Eq. (7). Here, we use the greedy search strategy to refine the correspondence of each driving point x_i^d by evaluating the regionwise similarity of each candidate location in a certain searching neighborhood. Since only a limited number of driving points are selected in our registration method, the computational speed is still fast.

After updating the correspondence on each driving point x_i^d, the dense deformation F can be estimated by fixing the latest updated correspondence field G and minimizing the last two terms in Eq. (7) (since the first similarity term is not related with F). Thus, it turns to the typical data fitting problem, i.e., interpolate the dense deformation field F based on the sparse correspondence field G. Considering all $\{x_i^d\}$ as

the source point (control point) set and $\{g(x_i^d)\}$ as the target point set, the thin-plate spline (TPS)[29] can be deployed here, which has the unified solution to minimize the bending energy as well as fit the results of correspondence detection $g(x_i^d)$ on the driving point x_i^d.

II.C.5. Constraint on tumor motion

Considering the physical property of tumor, tumor does not deform a lot during patient motion, compared with other normal breast tissues.[12,24] However, the deformable registration algorithms allow the free-form deformation on every point, which may result in unrealistic distortion on tumor. Therefore, it is important to consider the tumor region differently from the normal tissues during the registration, i.e., preserve its volume. Similar to the approach in Refs. 11 and 12, we first roughly extract the tumor region by detecting the intensity change over time, based on the observation that large contrast change usually occurs in tumor. Particularly, we calculate the maximum intensity change of MR signal between the precontrast image and all postcontrast images for each pixel as

$$\varepsilon(x) = \max_{i=1,\ldots,N} \frac{I_i(x) - I_0(x)}{I_0(x)}. \quad (8)$$

Then, the tumor region can be segmented by setting threshold on the values in the whole image, followed by some morphological operations. Next, the obtained regions are clustered by merging neighboring points to handle multiple tumor regions separately. The regions with a small number of points or very thin and long shape are not selected as tumor regions, in order to avoid inclusion of the enhanced nontumor regions, e.g., vessels.

The rigidity constraint on tumor deformation during registration can be well controlled by the nice property offered by TPS. For example, in TPS, the estimated displacement of each point is the weighted combination of global motion (guided by the affine transformation matrix of all image points) and the local deformation (guided by the parameters on TPS control points). Thus, we can enforce the rigidity constraint on tumor motion by raising the weight for global motion for each tumor point to suppress the local deformation. It is worth noting that the rigid transformation matrix for tumor is obtained by the least-square fitting from the correspondences of all driving points inside the extracted tumor region, instead of the entire driving point set, in order to more accurately measure tumor motion. The weights for global motion part are high inside the tumor mask and are gradually reduced to lower weights for the outside soft tissues. Figure 3 demonstrates the advantage of this strategy in registering a postcontrast image with a precontrast image [Fig. 3(a)]. Figures 3(b) and 3(c) display the deformation fields of tumor [the pink box in (a)] without and with the rigidity constraint, respectively. The tumor size becomes 94.9% of the original tumor size after using the rigidity constraint in (c), while it becomes only 70.1% without using the rigidity constraint (b). Therefore, it is clear that, when using the rigidity constraint, the tumor deformation is more reasonable.

II.D. Summary of our hierarchical registration framework

II.D.1. Summary of pairwise registration algorithm between two DCE-MR images

Given the template image T and subject image S, our pairwise registration algorithm can be briefly summarized below:

1. Perform the Canny edge detection on T and S, and get the boundary attribute a^{Bound}.
2. Calculate the local histogram-based attributes $\bar{a}^{\text{Hist}}$ for T and S.
3. Calculate the LSK-based attributes $\bar{a}^{LSK}$ for T and S.
4. Select the driving points for template T based on the a^{Bound}.
5. Determine the tumor region with Eq. (8).
6. Set the correspondence field G equal to the latest estimated deformation field F, i.e., $G \leftarrow F$.
7. For each driving point x_i^d, perform the greedy search in a certain neighborhood by evaluating the region-wise similarity w.r.t. each candidate in the subject image S.
8. Interpolate the dense deformation field F by TPS according to the correspondences on $\{x_i^d\}$.
9. Estimate the affine transformation in tumor region and enforce the rigid motion of tumor.
10. Smooth the deformation field to avoid the possible discontinuity between tumor and nontumor regions.
11. Relax the criterion on the boundary attribute a^{Bound} for selecting more driving points and go to step 6, until no more driving points can be added.

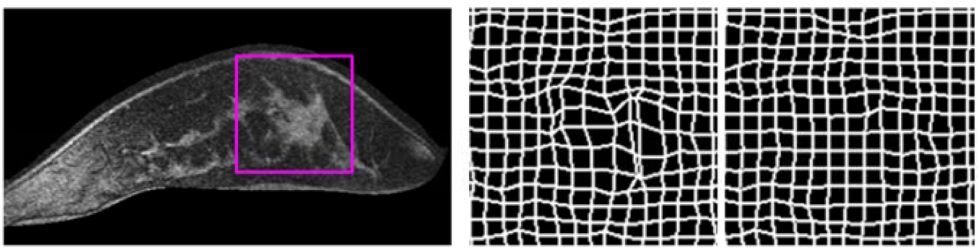

(a) pre-contrast image (b) without constraint (c) with constraint

FIG. 3. The advantage of rigidity constraint on tumor region. (b) and (c) show the deformations inside the box of tumor in (a), with and without rigidity constraint, respectively.

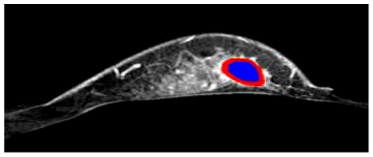

(a) Center area (blue) and boundary area (red) in tumor ROI

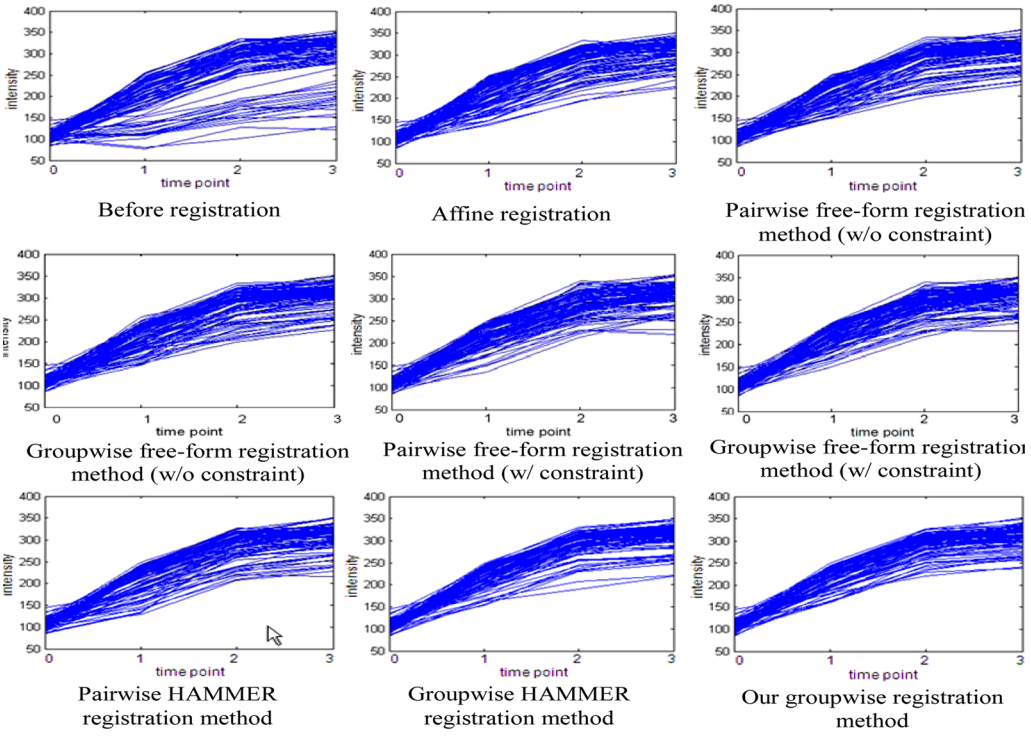

(b) Intensity enhancement curves for the points inside of tumor ROI (blue area in (a))

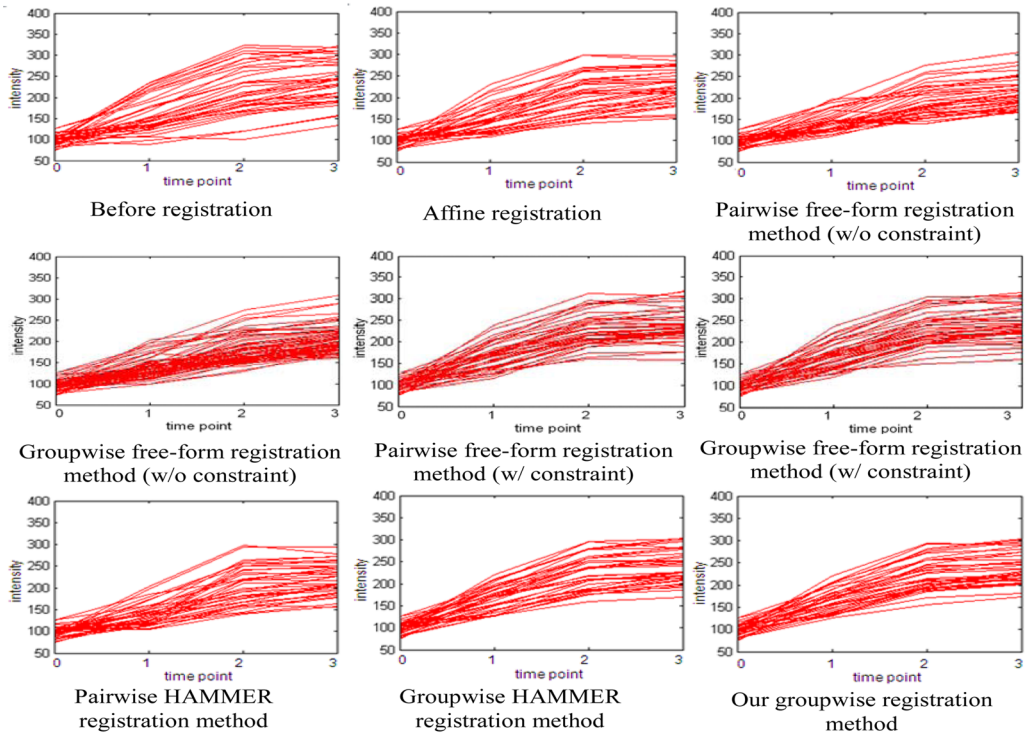

(c) Intensity enhancement curves for the boundary points of tumor ROI (red area in (a))

FIG. 4. The evolution of intensity in benign tumor region before registration and after registration by eight registration methods. It can be observed that our method achieves more consistent registration result than all other methods, in both uniform tumor region and tumor boundary.

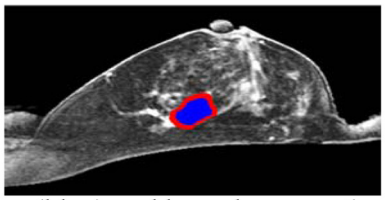

(a) Center area (blue) and boundary area (red) in tumor ROI

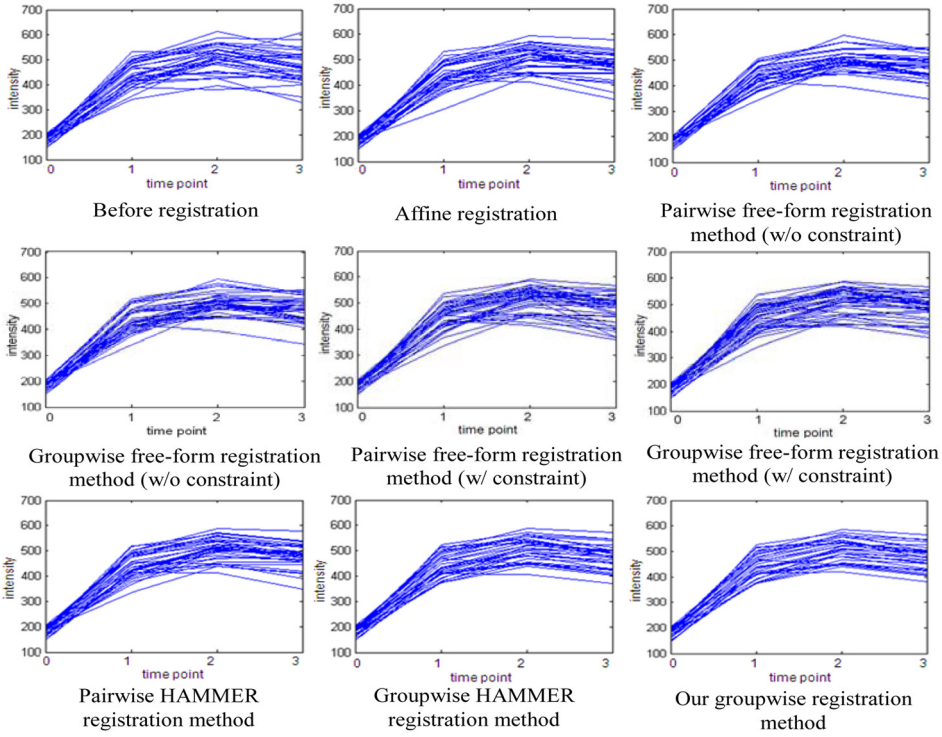

(b) Intensity enhancement curves for the points inside of tumor ROI (blue area in (a))

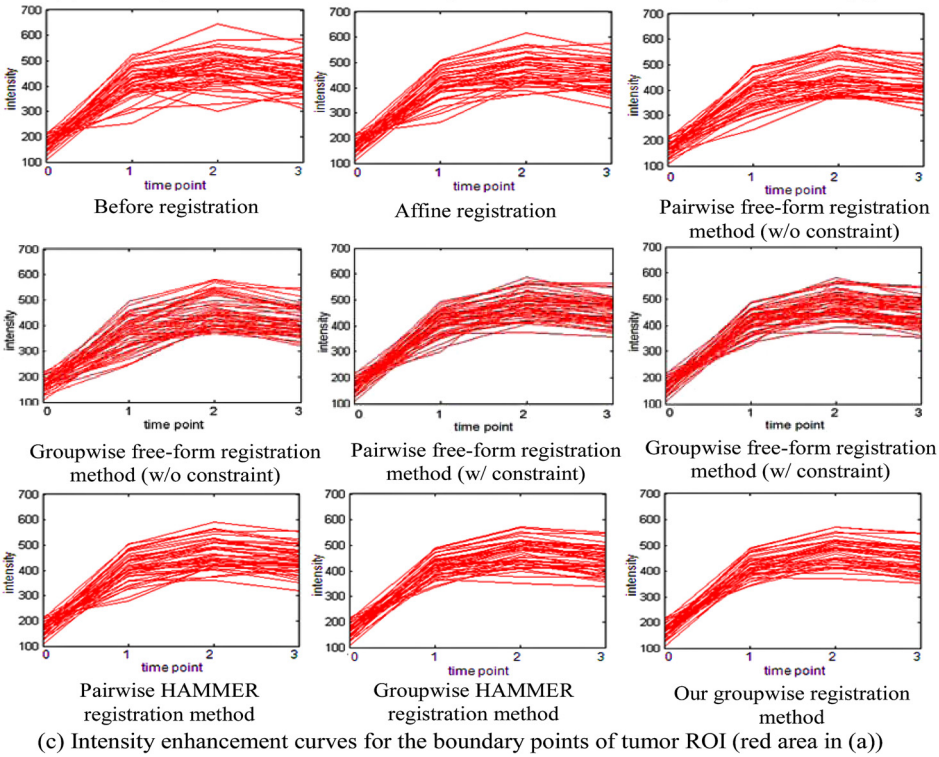

(c) Intensity enhancement curves for the boundary points of tumor ROI (red area in (a))

FIG. 5. The evolution of intensity in the malignant tumor region before registration and after registration by eight registration methods. It can be observed that our method achieves more consistent registration result than any other methods, especially along tumor boundary.

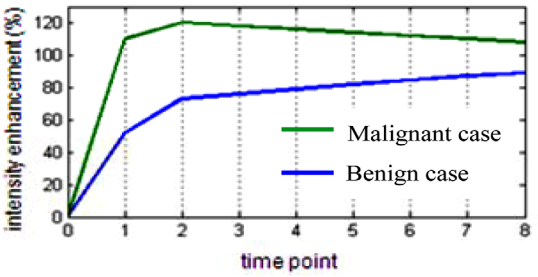

FIG. 6. Simulated intensity enhancement curves for the malignant tumor (upper one) and benign tumor (lower one). The percentage of intensity enhancement of post-contrast image at different time points (between 1 and 8) is computed relative to the pre-contrast image (time point 0).

II.D.2. Summary of hierarchical registration algorithm for whole DCE-MR images

Given the precontrast image I_0 and several postcontrast images $I_t(t = 1, \ldots, N)$, our hierarchical registration method for whole DCE-MR image is performed with the following steps:

1. Groupwise registration for all postcontrast images (SP_1).
   (a) Estimate the group-mean image M according to the currently registered postcontrast images [by Eq. (1)].
   (b) Register all postcontrast images with the group-mean image obtained in step 1.1 and get the deformation field $F_{M \to I_t}$ (by using our pairwise registration algorithm proposed in Sec. II C).
   (c) If not converged, go to step 1.1.
2. Register the group-mean image M of all postcontrast images with the precontrast image I_0 (SP_2).
3. Compute the final deformation F_t for each postcontrast image I_t by composing the deformation field $F_{M \to I_t}$ with $F_{I_0 \to M}$.

III. EXPERIMENTAL RESULTS

Our proposed registration method has been extensively evaluated on both real and simulated breast DCE-MR images. The performance of our registration method is compared with affine registration (FSL package[31]), and three pairwise registration methods: (1) pairwise free-form (B-spline-based) registration method without volume-preserving constraint,[5] (2) pairwise free-form registration method with volume-preserving constraint, and (3) pairwise (feature-based) HAMMER registration method.[20] In order to specifically evaluate the proposed registration method for breast DCE-MRI registration in Sec. II C, we further integrate the free-form registration method with or without

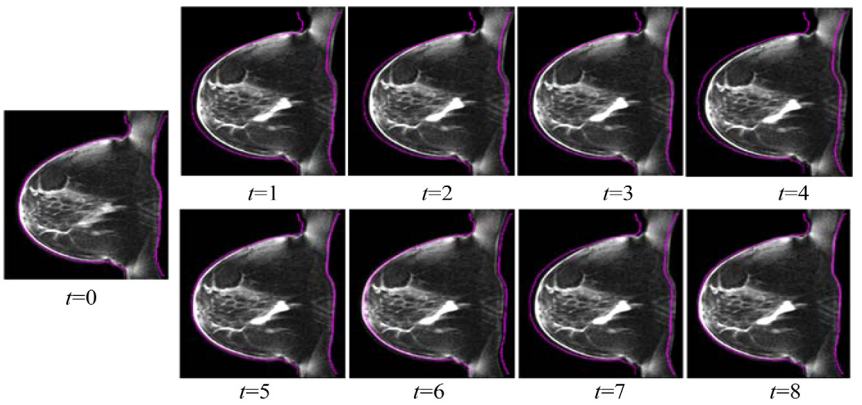

(a) simulated benign post-contrast images (t=1…8) by applying the intensity enhancement model of benign tumor to a pre-contrast image

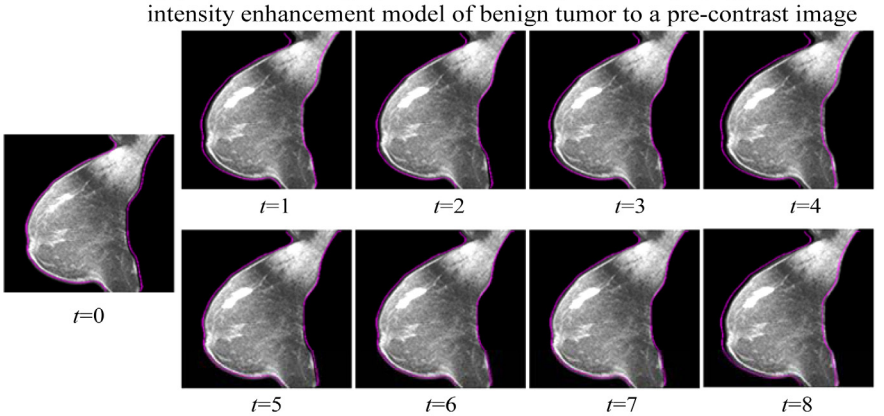

(b) simulated malignant post-contrast images (t=1…8) by applying the intensity enhancement model of malignant tumor to a pre-contrast image

FIG. 7. Simulated benign (a) and malignant (b) tumor images according to the intensity enhancement curves given in Fig. 6 and the simulated global transformation and local B-spline based deformation field. To show the amount of breast motion at different time points compared to the pre-contrast image, the contour from pre-contrast image (t=0) is overlaid onto all post-contrast images at different time points (t=1…8).

volume-preserving constraint and the HAMMER registration method into our groupwise registration framework, thus called the groupwise free-form registration without volume-preserving constraint, the groupwise free-form registration with volume-preserving constraint, and the groupwise HAMMER registration, respectively. For all free-form registration methods, the third-order B-spline function with the control point spacing of 20 mm is used. For all of the following experiments, we use the same set of parameters for each method.

Dataset: The images used in our experiments are the T2-weighted DCE-MR images acquired from ten subjects, with five subjects having malignant tumor and five subjects having benign tumor. The temporal resolution is 45 s, i.e., the DCE-MR images were acquired every 45 s after injecting agent, with totally 4–9 images acquired. The images size and resolution range from 384×384 with 0.47×0.47 mm^2 to 896×896 with 0.22×0.22 mm^2, depending on the imaging scanners used. Background and chest wall area are removed before performing registration.

III.A. Experiments on real dataset

III.A.1. Evaluation on benign case

We evaluate the registration accuracy in aligning the postcontrast images to the precontrast image, by visual inspection on a benign tumor case. Since the contrast agent takes effect to all tumor points homogeneously in precontrast and postcontrast stages for the example we used in this experiment, the intensity change of tumor points should be continuous and consistent over time. Therefore, Fig. 4 shows the estimated evolution curve of intensity in the benign tumor region [Fig. 4(a)], from the precontrast image ($t = 0$) to all warped postcontrast images ($t = 1,2,3$). Especially, we evaluate at the tumor boundary [red in Fig. 4(a)] and inside uniform regions [blue in Fig. 4(a)] separately. From left to right and top to bottom, Fig. 4(b) shows the estimated intensity evolution curves of internal tumor points before registration and after registration by affine registration, pairwise free-form registration without volume-preserving constraint, groupwise free-form registration without volume-preserving

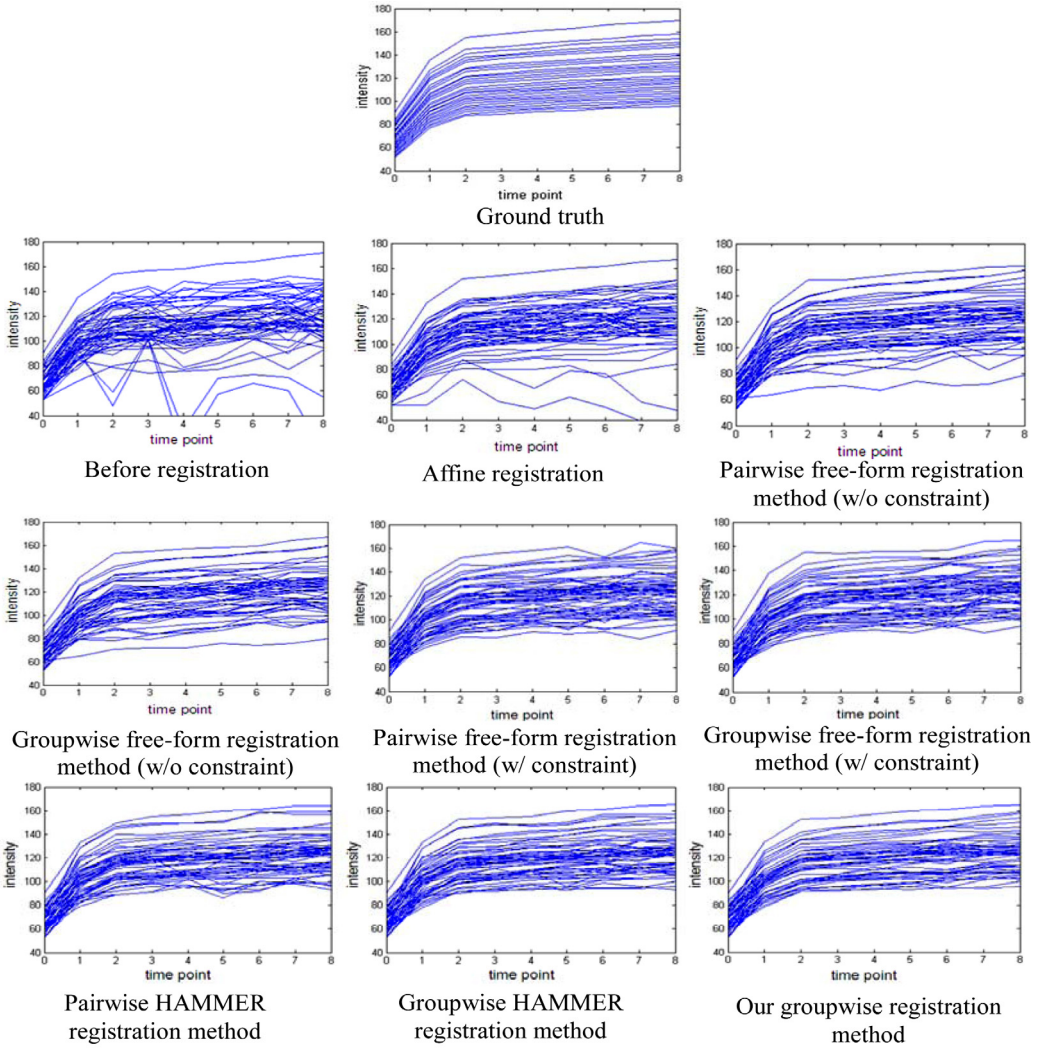

(a) intensity enhancement curves for ROI of benign tumor image

FIG. 8. The evolution of intensity in the simulated benign (a) and malignant (b) tumor regions before registration and after registration by eight methods. It can be observed that our method achieves more consistent registration result than all other methods.

constraint, pairwise free-form registration with volume-preserving constraint, groupwise free-form registration with volume-preserving constraint, pairwise HAMMER registration, groupwise HAMMER registration, and our registration method, respectively. Following the same order, Fig. 4(c) shows the intensity evolution curves of points at tumor boundary before and after registration by different registration methods. It can be observed that the longitudinal intensity changes of tumor points after registration is much more consistent by our method than by all other methods, in both uniform region [Fig. 4(b)] and tumor boundary [Fig. 4(c)].

III.A.2. Evaluation on malignant case

Similarly, Fig. 5 shows the temporal intensity change at a tumor region, for a typical malignant case. Again, our registration method outperforms all other methods in terms of registration consistency. It is worth noting that the characteristics of estimated intensity evolution curves on both benign and malignant cases (i.e., the pattern of intensity changes) are well matched with the agent wash-in/wash-out curves described in the clinical literatures.[1,2]

III.B. Experiments on simulated dataset

Due to the lack of ground truth in real data, we generate the simulated data to validate the registration accuracy by considering both breast deformation and contrast changes. To achieve it, we manually delineated tumor ROI on the postcontrast image (with maximum intensity enhancement) by an expert. This ROI is then warped onto the precontrast image to extract tumor ROI in the precontrast image space. After this, we use the following two steps to simulate a series of new postcontrast images for each simulated subject. *First*, we simulate the evolution of contrast change at each pixel of the precontrast image to generate a set of postcontrast images over time, without geometric deformation at this stage. Specifically, the evolution of contrast change for benign and malignant tumor[2] is learned from real cases, with examples shown in Fig. 6. For points inside the tumor

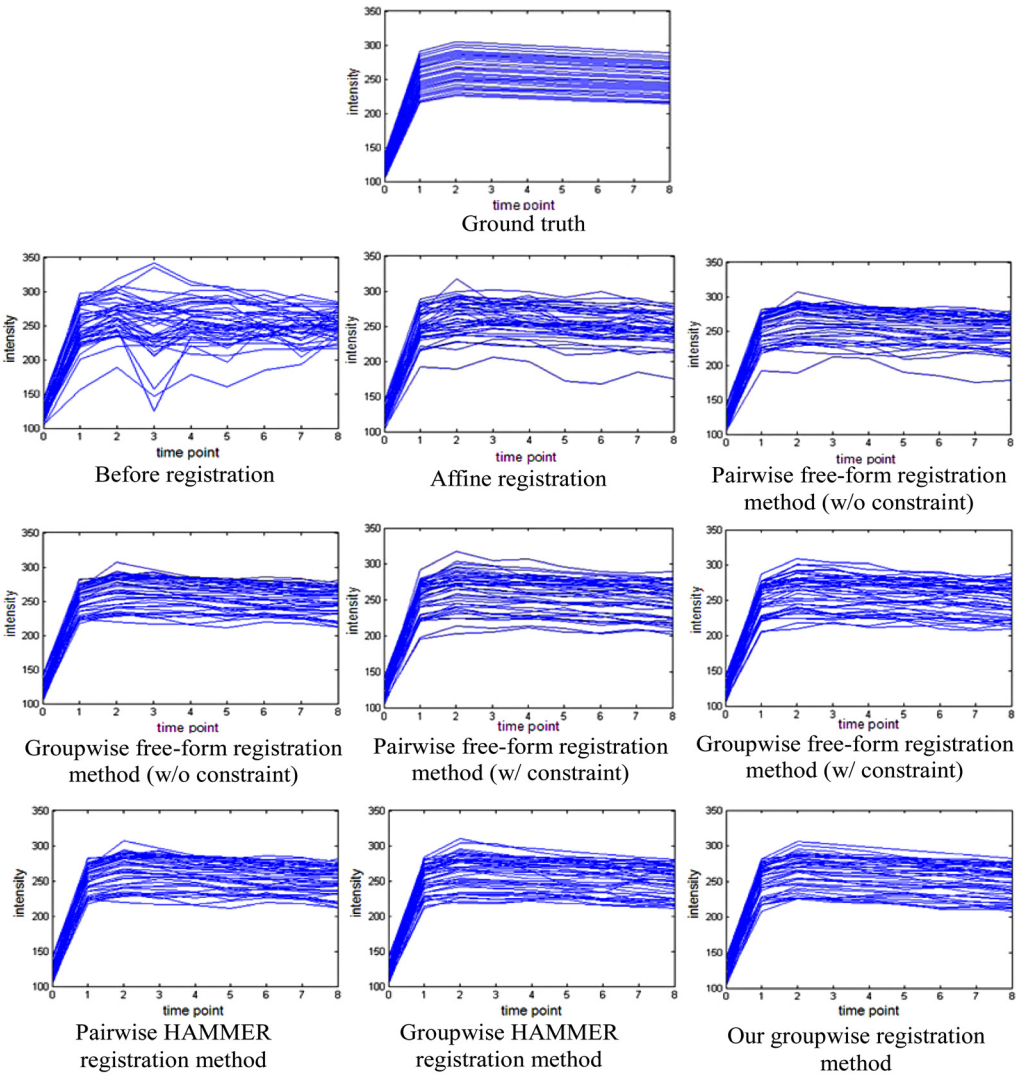

(b) intensity enhancement curves for ROI of malignant tumor image

FIG. 8. (*Continued*)

region, the intensity is increased according to the intensity evolution curve as shown in Fig. 6. Since normal tissues are also enhanced by the contrast agent but much less than tumor, we also simulate this effect in our data. In this way, we can generate contrast-enhanced images with higher enhancement in the tumor ROI and lower enhancement in the normal tissues. *Second*, we simulate breast deformation for each of the above-simulated contrast-enhanced images as follows. (1) We use a conventional registration method, e.g., mutual-information-based registration method,[5] to compute the deformation field between each pair of postcontrast and precontrast images, for all ten subjects. (2) We estimate the B-spline parameters from these deformation fields, as well as the magnitude of breast deformation, i.e., ~4 mm. (3) We perturb each B-spline parameter for a certain amount (up to 4 mm), and then reconstruct the dense deformation fields from these simulated B-spline parameters. (4) We generate the final postcontrast images by deforming the previous-simulated contrast-enhanced images (in the first step) with the simulated deformation fields. Note that we apply only rigid transformation to tumor ROIs, while applying the simulated deformations to other areas. This can preserve tumor volume over time in the simulated images. Figure 7 shows the typical simulated postcontrast images for the benign (a) and malignant cases (b), respectively.

To evaluate the registration performance, we register the simulated images in Fig. 7 to the precontrast image by affine registration, pairwise/groupwise free-form registration with and without volume-preserving constraint, pairwise/groupwise HAMMER, and our groupwise registration methods. Figure 8 shows the estimated curves of intensity change in the tumor area for all warped postcontrast images ($t = 1 \ldots 8$), with benign case in (a) and malignant case in (b). Compared with the ground truth [the curve displayed on the top of Figs. 8(a) and 8(b), respectively], the estimated intensity evolution curves by our groupwise registration methods are visually much closer to the ground truth and smoother over time than all other registration methods. To quantitatively evaluate each registration method, we can further compute the average distance between the ground-truth intensity evolution curves and their corresponding curves estimated by each registration method. The distance for the benign tumor case [Fig. 8(a)] is 1.49 mm before registration, 1.09 mm by affine registration, 0.95 mm by pairwise unconstrained free-form registration (FFD), 0.92 mm by groupwise unconstrained FFD, 0.91 mm by pairwise constrained FFD, 0.86 mm by groupwise constrained FFD, 0.8 mm by pairwise HAMMER, 0.7 mm by groupwise HAMMER, and 0.66 mm by our registration method, respectively. Similarly, the distance for the malignant case [Fig. 8 (b)] is 1.35 mm before registration, 0.93 mm by affine registration, 0.85 mm by pairwise unconstrained FFD, 0.81 mm by groupwise unconstrained FFD, 0.74 mm by pairwise constrained FFD, 0.7 mm by groupwise constrained FFD, 0.67 mm by pairwise HAMMER, 0.62 mm by groupwise HAMMER, and 0.58 mm by our registration method, respectively. It is clear that our registration method achieves the best registration performance among all methods under comparison.

Given the ground-truth deformation field, we can also calculate the voxelwise residual errors between the ground-truth deformation fields and the deformation fields estimated by each of the eight registration methods. The mean and maximum residual errors by affine registration,

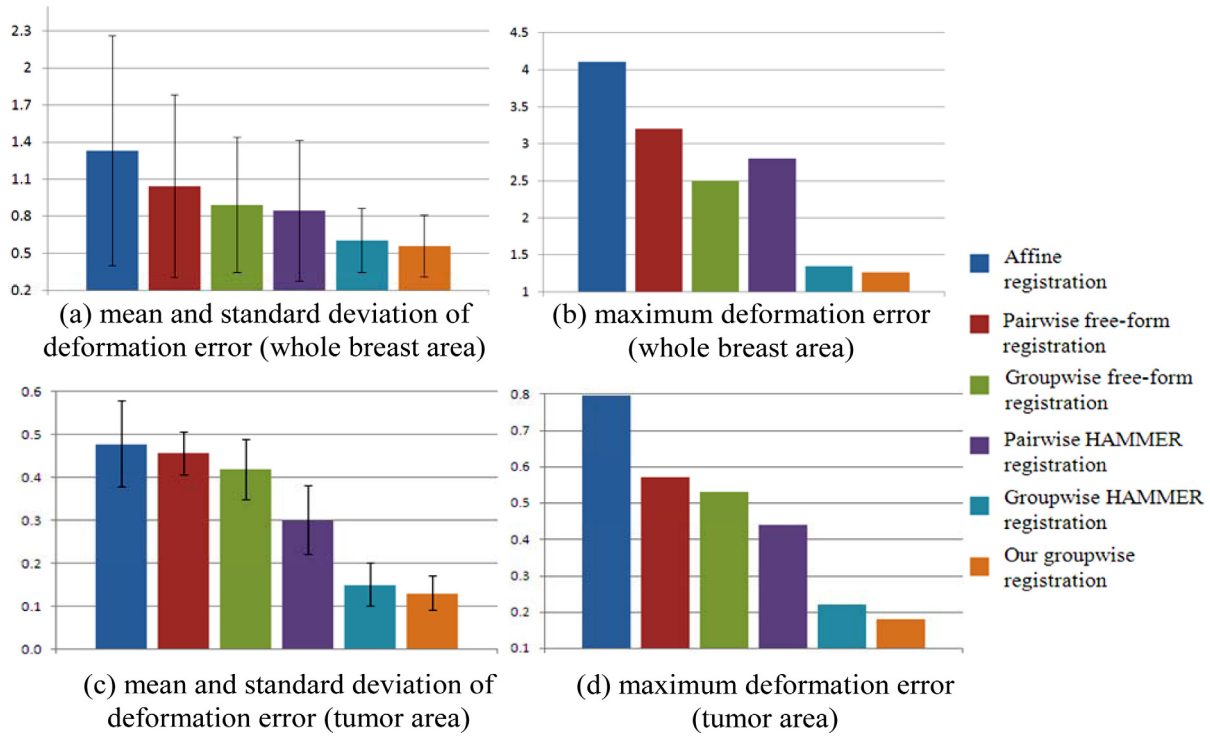

FIG. 9. Top: The mean (a) and maximum (b) deformation estimation errors in the whole breast; Bottom: The mean (c) and maximum (b) deformation estimation errors in the tumor by six registration methods.

pairwise/groupwise unconstrained free-form registration, pairwise/groupwise HAMMER registration, and our groupwise registration methods are shown in Fig. 9. Note that the results by the constrained free-form registration methods are not reported here, since the related software package[32] does not provide the explicit deformation fields. As shown in Fig. 9, it can be confirmed that our method again achieves the best performance in estimating accurate breast motion.

IV. CONCLUSION

In this paper, we have proposed a novel groupwise registration method to achieve accurate and consistent alignment for breast DCE-MR images. The simultaneous alignment of postcontrast images to a precontrast image via a group-mean greatly improves the registration consistency of the postcontrast images. The attribute vectors, which consist of local histogram- and local steering kernel-based features, are utilized to obtain robust anatomical correspondences in case of dramatic contrast change and image noise. In order to reduce the unrealistic deformation in tumor region, we adaptively treat motion of tumor as rigid in the proposed framework while allowing other soft tissues to follow the deformable motion. The registration performance of the proposed method has been evaluated in both real and simulated data, by comparison with various pairwise/groupwise registration methods. In all experiments, our proposed method achieves the best performance in both registration accuracy and registration consistency. In the future, we will further evaluate our proposed method on more real images with various tumor patterns and make it applicable for the clinical study.

ACKNOWLEDGMENT

This work was supported by NIH Grant No. 1R21 CA140841, The National Basic Research Program of China (973 Program) No. 2010CB732505, and NSFC Grant No. 61075010.

[a]Author to whom correspondence should be addressed. Electronic mail: dgshen@med.unc.edu; Telephone: 9199663535; Fax: 9198432641.

[1]N. Hylton, "Dynamic contrast-enhanced magnetic resonance imaging as an imaging biomarker," J. Clin. Oncol. **24**, 3293–3298 (2006).
[2]W. Chen, M. L. Giger, L. Lan, and U. Bick, "Computerized interpretation of breast MRI: Investigation of enhancement-variance dynamics," Med. Phys. **31**, 1076–1082 (2004).
[3]R. Kumar, J. C. Asmuth, K. Hanna, J. R. Bergen, C. Hulka, D. B. Kopans, R. Weisskoff, and R. H. Moore, "Application of 3D registration for detecting lesions in magnetic resonance breast scans," *SPIE Medical Imaging* (SPIE, Newport Beach, 1996), pp. 646–656.
[4]P. Hayton, M. Brady, L. Tarassenko, and N. Moore, "Analysis of dynamic MR breast images using a model of contrast enhancement," Med. Image Anal. **1**, 207–224 (1997).
[5]D. Rueckert, L. I. Sonoda, C. Hayes, D. L. G. Hill, M. O. Leach, and D. J. Hawkes, "Non-rigid registration using free-form deformations: Application to breast MR images," IEEE Trans. Med. Imaging. **18**, 712–721 (1999).
[6]Y. Sun, C. Yan, S.-H. Ong, E. Tan, and S.-C. Wang, "Intensity-based volumetric registration of contrast-enhanced MR breast images," *Medical Image Computing and Computer-Assisted Intervention – MICCAI 2006* Springer, (Berlin/Heidelberg, 2006), Vol. 4190, pp. 671–678.
[7]E. R. E. Denton, L. I. Sonoda, D. Rueckert, S. C. Rankin, C. Hayes, M. O. Leach, D. L. G. Hill, and D. J. Hawkes, "Comparison and evaluation of rigid, affine, and nonrigid registration of breast MR images," J. Comput. Assist. Tomogr. **23**, 800–805 (1999).
[8]W. R. Crum *et al.*, "Anisotropic multi-scale fluid registration: Evaluation in magnetic resonance breast imaging," Phys. Med. Biol. **50**, 5153 (2005).
[9]T. Bruckner, R. Lucht, and G. Brix, "Comparison of rigid and elastic matching of dynamic magnetic resonance mammographic images by mutual information," Med. Phys. **27**, 2456–2461 (2000).
[10]J. A. Schnabel, C. Tanner, A. D. Castellano-Smith, A. Degenhard, C. Hayes, M. O. Leach, D. R. Hose, D. L. Hill, and D. J. Hawkes, "Finite-element based validation of nonrigid registration using single- and multilevel free-form deformations: Application to contrast-enhanced MR mammography," *SPIE Medical Imaging 2002* (San Diego, CA, 2002) pp. 550–561.
[11]C. Tanner, J. A. Schnabel, D. Chung, M. J. Clarkson, D. Rueckert, D. L. G. Hill, and D. J. Hawkes, "Volume and shape preservation of enhancing lesions when applying non-rigid registration to a time series of contrast enhancing MR breast images," *Medical Image Computing and Computer-Assisted Intervention – MICCAI* (Springer, Berlin/Heidelberg, 2000), Vol. 1935, pp. 327–337.
[12]T. Rohlfing, C. R. MaurerJr., D. A. Bluemke, and M. A. Jacobs, "Volume-preserving nonrigid registration of MR breast images using free-form deformation with an incompressibility constraint," IEEE Trans. Med. Imaging **22**, 730–741 (2003).
[13]M. H. Paul, B. Michael, M. S. Stephen, and M. Niall, "A non-rigid registration algorithm for dynamic breast MR images," Artif. Intelligence **114**, 125–156 (1999).
[14]M. Ebrahimi and A. Martel, "A general PDE-framework for registration of contrast enhanced images," *Medical Image Computing and Computer-Assisted Intervention – MICCAI2009* (Springer-Verlag, Berlin/Heidelberg, 2009).
[15]J. Lo, M. Brady, and N. Moore, "Simultaneous multiple image registration method for T1 estimation in breast MRI images," in *Medical Image Computing and Computer-Assisted Intervention – MICCAI 2006* (Springer, Berlin, Heidelberg, 2006), Vol. 4190, pp. 865–872.
[16]Y. Zheng, J. Yu, C. Kambhamettu, S. Englander, M. D. Schnall, and D. Shen, "De-enhancing the dynamic contrast-enhanced breast MRI for robust registration," *Medical Image Computing and Computer-Assisted Intervention – MICCAI 2007*, Brisbane, Australia, 2007.
[17]Y. Zheng, A. D. A. Maidment, and J. C. Gee, "Accurate registration of dynamic contrast-enhanced breast MR images with robust estimation and linear programming," *Proceedings of the 2010 IEEE International Conference on Biomedical Imaging: From Nano to Macro* (IEEE Press, Rotterdam, The Netherlands, 2010).
[18]H. Takeda, S. Farsiu, and P. Milanfar, "Kernel regression for image processing and reconstruction," IEEE Trans. Image Process. **16**, 349–366 (2007).
[19]H. Seo and P. Milanfar, "A non-parametric approach to automatic change detection in MRI images of the brain," *IEEE International Symposium on Biomedical Imaging: From Nano to Macro (ISBI)* (IEEE press, Boston, MA, 2009), pp. 245–248.
[20]D. Shen, "Image registration by local histogram matching," Pattern Recognit. **40**, 1161–1171 (2007).
[21]J. Ashburner, "Computational neuroanatomy," Ph.D. thesis, University College London, 2000.
[22]J. A. Little, D. L. G. Hill, and D. J. Hawkes, "Deformations Incorporating Rigid Structures", Computer Vision and Image Understanding, (Elsevier Science Inc., San Francisco, CA, 1997), Vol. 66, pp. 223–232.
[23]S. Marius *et al.*, "Nonrigid registration with tissue-dependent filtering of the deformation field," Phys. Med. Biol. **52**, 6879 (2007).
[24]C. Tanner, J. A. Schnabel, D. L. G. Hill, D. J. Hawkes, A. Degenhard, M. O. Leach, D. R. Hose, M. A. Hall-Craggs, and S. I. Usiskin, "Quantitative evaluation of free-form deformation registration for dynamic contrast-enhanced MR mammography," Med. Phys. **34**, 1221–1233 (2007).
[25]X. Li, B. M. Dawant, E. B. Welch, A. B. Chakravarthy, D. Freehardt, I. Mayer, M. Kelley, I. Meszoely, J. C. Gore, and T. E. Yankeelov, "A nonrigid registration algorithm for longitudinal breast MR images and the analysis of breast tumor response," Magn. Reson. Imaging **27**, 1258–1270 (2009).
[26]H. Fischer, M. Otte, C. Ehritt-Braun, J. Laubenberger, and J. Hennig, "Local elastic matching and pattern recognition in MR mammography," Int. J. Imaging Syst. Technol. **10**, 199–206 (1999).

[27]J. Canny, "A computational approach to edge detection," IEEE Trans. Pattern Anal. Machine Intelligence **8**, 679–698 (1986).
[28]D. Shen and C. Davatzikos, "HAMMER: Hierarchical attribute matching mechanism for elastic registration," IEEE Trans. Med. Imaging, **21** 1421–1439 (2002).
[29]G. Wu, P.-T. Yap, M. Kim, and D. Shen, "TPS-HAMMER: Improving HAMMER registration algorithm by soft correspondence matching and thin-plate splines based deformation interpolation," Neuroimage **49**, 2225–2233 (2010).
[30]H. Chui and A. Rangarajan, "A new point matching algorithm for non-rigid registration," Comput. Vis. Image Underst. **89**, 114–141 (2003).
[31]S. M. Smith, M. Jenkinson, M. W. Woolrich, C. F. Beckmann, T. E. J. Behrens, H. Johansen-Berg, P. R. Bannister, M. D. Luca, I. Drobnjak, D. E. Flitney, R. Niazy, J. Saunders, J. Vickers, Y. Zhang, N. D. Stefano, J. M. Brady, and P. M. Matthews, "Advances in functional and structural MR image analysis and implementation as FSL," Neuroimage **23**, 208–219 (2004).
[32]www.doc.ic.ac.uk/∼dr/software/.